Eddy-Length-Scale Response to Static Stability Change in an Idealized Dry Atmosphere: A Linear Response Function Approach

PAK WAH CHAN, a PEDRAM HASSANZADEH, b,c AND ZHIMING KUANG a,d

^a Department of Earth and Planetary Sciences, Harvard University, Cambridge, Massachusetts
 ^b Department of Mechanical Engineering, Rice University, Houston, Texas
 ^c Department of Earth, Environmental and Planetary Sciences, Rice University, Houston, Texas
 ^d John A. Paulson School of Engineering and Applied Sciences, Harvard University, Cambridge, Massachusetts

(Manuscript received 17 February 2021, in final form 19 May 2021)

ABSTRACT: The response of midlatitude equilibrated eddy length scale to static stability has long been questioned but not investigated in well-controlled experiments with unchanged mean zonal wind and meridional temperature gradient. With iterative use of the linear response function of an idealized dry atmosphere, we obtain a time-invariant and zonally uniform forcing to decrease the near-surface temperature by over 2 K while keeping the change in zonal wind negligible (within $0.2 \,\mathrm{m\,s^{-1}}$). In such experiments of increased static stability, energy-containing zonal scale decreases by 3%-4%, which matches with Rhines scale decrease near the jet core. Changes in Rossby radius (+2%), maximum baroclinic growth scale (-1%), and Kuo scale (0%) fail to match this change in zonal scale. These findings and well-controlled experiments help with better understanding of eddy-mean flow interactions and hence the midlatitude circulation and its response to climate change.

SIGNIFICANCE STATEMENT: In the midlatitude atmosphere, eddy size is the length scale of the prevalent weather systems and has important implications for midlatitude temperature variability and jet shift. We want to understand how it changes with increased static stability (a measure of vertical temperature gradient). We manage to isolate an increase in static stability, without changing the north–south temperature gradient. Our idealized and well-controlled simulation shows that eddy size decreases with increased static stability. This decrease matches quantitatively with a nonlinear scaling argument, but does not support linear scaling arguments involving instability of vertical wind shear or horizontal wind shear. This helps with theoretical understanding of eddy–mean flow interactions and hence the midlatitude circulation and its response to climate change.

KEYWORDS: Atmospheric circulation; Eddies; Rossby waves; Stability; Wave properties; Jets; General circulation models; Idealized models; Spectral analysis/models/distribution

1. Introduction

Eddies play a key role in shaping the midlatitude atmospheric circulation and climate. They are often generated near the midlatitude jet stream, where there is strong meridional temperature gradient and strong vertical wind shear, and propagate meridionally outward from the jet in the upper troposphere. By doing so, they converge westerly momentum and thus maintain the jet. At the same time, eddies transport heat poleward and thereby act to reduce the meridional temperature gradient.

Length scale is one of the important aspects of eddies. This is the length scale of the prevalent weather systems we observe in the midlatitudes. On the one hand, eddy length scale sets the mixing length, which governs the midlatitude temperature variability (e.g., Schneider et al. 2015). On the other hand, eddy length scale determines the intrinsic zonal phase speed of eddies via the Rossby wave's dispersion relationship,

Chan's current affiliation: College of Engineering, Mathematics and Physical Sciences, University of Exeter, Exeter, United Kingdom.

Corresponding author: Pak Wah Chan, pchan@g.harvard.edu

 $c-\overline{u}=-\beta/(k^2+l^2)$, where c is the zonal phase speed, \overline{u} is the mean zonal wind, β is the gradient of the Coriolis parameter, and k and l are the wavenumbers in the zonal and meridional directions. For mean states that are zonally homogeneous and time invariant, c is conserved. When the waves propagate outward from the jet to latitudes with weaker \overline{u} , $c-\overline{u}$ may no longer be negative and the waves will break at this latitude, referred to as the critical latitude. Therefore, a larger length scale, or a smaller wavenumber, will give a more negative (eastward) intrinsic phase speed and thus may allow the waves to propagate further outward from the jet. Based on how the eddy length scale sets the critical latitude of eddies, studies (e.g., Kidston et al. 2011) have proposed that increased eddy length scale under global warming can cause a poleward shift of the jet.

Over years, some theories have been proposed to explain the length scale of eddies. In the linear baroclinic instability problem of Eady, the most unstable mode has its length scale proportional to the Rossby internal radius of deformation,

$$L_D = \frac{NH}{f},\tag{1}$$

where N is the buoyancy frequency (static stability), H is the depth of the fluid, and f is the Coriolis parameter. In the

DOI: 10.1175/JAS-D-21-0044.1

Charney problem, the H in this formula is replaced by the depth of the eddies, which is limited by the scale height. In application to the atmosphere, H in the Rossby radius is often taken as the tropopause height, but sometimes also taken as the pressure scale height (Frierson et al. 2006).

An extension within the linear argument is to consider the nonuniform profile of static stability and vertical wind shear. One can discretize the atmosphere in multiple vertical levels, and numerically solve the quasigeostrophic (QG) eigenvalue problem to compute the most unstable baroclinic mode and its wavenumber (Smith 2007; Pfahl et al. 2015; Kang et al. 2019).

Nonlinear turbulent theory, on the other hand, suggests that energy will cascade to larger length scale, until it is halted by β . The resulting energy-containing length scale will be proportional to the Rhines scale,

$$L_{\beta} = \left(\frac{\text{EKE}^{1/2}}{\beta}\right)^{1/2},\tag{2}$$

where EKE is the eddy kinetic energy (Rhines 1975). The Kuo scale.

$$L_K = \left(\frac{\overline{u}_{\text{max}}}{\beta}\right)^{1/2},\tag{3}$$

looks similar to the Rhines scale and is called Rhines scale in some studies (e.g., Farrell and Ioannou 2007), but the two scales are dynamically different (Vallis 2006; Nabizadeh et al. 2019). The Kuo scale might be less relevant for Earth, in the sense that it has only one midlatitude westerly jet on each hemisphere. Whereas if there are alternating easterlies and westerlies, the Kuo scale will set the minimum width of a stable easterly jet (Rayleigh–Kuo inflection point criterion; Farrell and Ioannou 2007; Vallis 2006). The jet width set by the Kuo scale will then set the eddy length scale (Chemke and Kaspi 2016). We include the Kuo scale for the sake of completeness, and to help clarify our definition of "Rhines scale."

The applicability of these length scale arguments, especially of the Rossby radius and the Rhines scale, has been tested in different models and different setups in the past few decades.

In a two-layer QG model, the Rhines scale is found to match well with the eddy length scale when the bottom drag is weak (e.g., Panetta 1993; Held and Larichev 1996; Thompson and Young 2007). In idealized moist general circulation models (GCMs), the Rhines scale is also found to match well with the eddy length scale, when moisture content is varied (Frierson et al. 2006), rotational rate is varied (Chemke and Kaspi 2016), or when different forcings and boundary conditions are applied (Barry et al. 2002). In between, for an idealized dry GCM, Schneider and Walker (2006) argued that both the Rhines scale and the Rossby radius will fit well with the eddy length scale and it is difficult to separate the two. On the contrary, some later studies (e.g., Zurita-Gotor 2008; Jansen and Ferrari 2012) found the Rhines scale and the Rossby radius to be separable and that the Rhines scale fits the eddy length scale better.

Some studies, however, dismissed the applicability of the Rhines scale in describing the eddy length scale in the atmosphere. In Coupled Model Intercomparison Project, phase 3

(CMIP3), by doing an intermodel correlation, Kidston et al. (2010) found the increase of eddy length scale in the twentyfirst century to well correlate with the increase in static stability (N) between 850 and 600 hPa, but they did not find the increase in length scale to correlate with EKE or magnitude of the poleward shift of jet (surrogate for β). In CMIP3, reanalysis and dry GCM, by regressing internal variability on southern annular mode (surrogate of jet shift), Kidston et al. (2011) also found that the shift of jet and EKE have shortcomings in explaining the variability of length scale, but static stability (N)between 800 and 500 hPa to be consistent with the variations of length scale. Kidston et al. (2011) also conducted an experiment of increased N in an idealized dry GCM, where they found increase in eddy length scale. This experiment was originally meant to test if increase of length scale can allow waves to propagate further from the jet and therefore cause the jet to shift poleward. They noted that, unfortunately, the increased N came with increased meridional temperature gradient, and the influence of N and meridional temperature gradient became somewhat inseparable.

With a recent technique of linear response function (LRF; Hassanzadeh and Kuang 2016), we can now change the static stability without changing meridional temperature gradient in a dry GCM. While these experiments are idealized and do not necessarily resemble global-warming scenarios, they are essential for a better theoretical understanding of the response of eddies to the mean state. As we will see in later sections, experiments of increased *N* will give us weaker EKE and thus a smaller Rhines scale. We can then test how the Rossby radius, the Rhines scale, and other length scale arguments work in a dry GCM in the context of sole change in static stability.

2. Methods

a. Dry GCM ensemble

We use the GFDL dry spectral dynamical core with Held and Suarez (1994) forcing. The setup is identical to that of Hassanzadeh and Kuang (2016) with T63 spectral resolution and 40 vertical levels. Each ensemble consists of 20 runs with slightly different initial conditions, and each run is 26 000 days with daily snapshots (first 1000 days discarded). The two hemispheres are symmetrically forced, so we present the aggregated results. Each ensemble will then have 1 000 000 days of valid data. Such large ensemble size and long simulation allow us to have small uncertainty in the meridional temperature gradient.

b. Forced experiments

The following ensemble experiments are conducted in comparison to the above control ensemble experiment:

K11: This experiment increases the static stability by applying the forcing in the $N_{\rm increased}$ experiment in Kidston et al. (2011). The equilibrium temperature ($T_{\rm eq}$) field in the Newtonian relaxation is decreased by 3 K at $\sigma > 0.85$, where σ is pressure divided by surface pressure. Changing $T_{\rm eq}$ is equivalent to a temperature forcing in kelvins per day, as converted by the Newtonian relaxation rate.

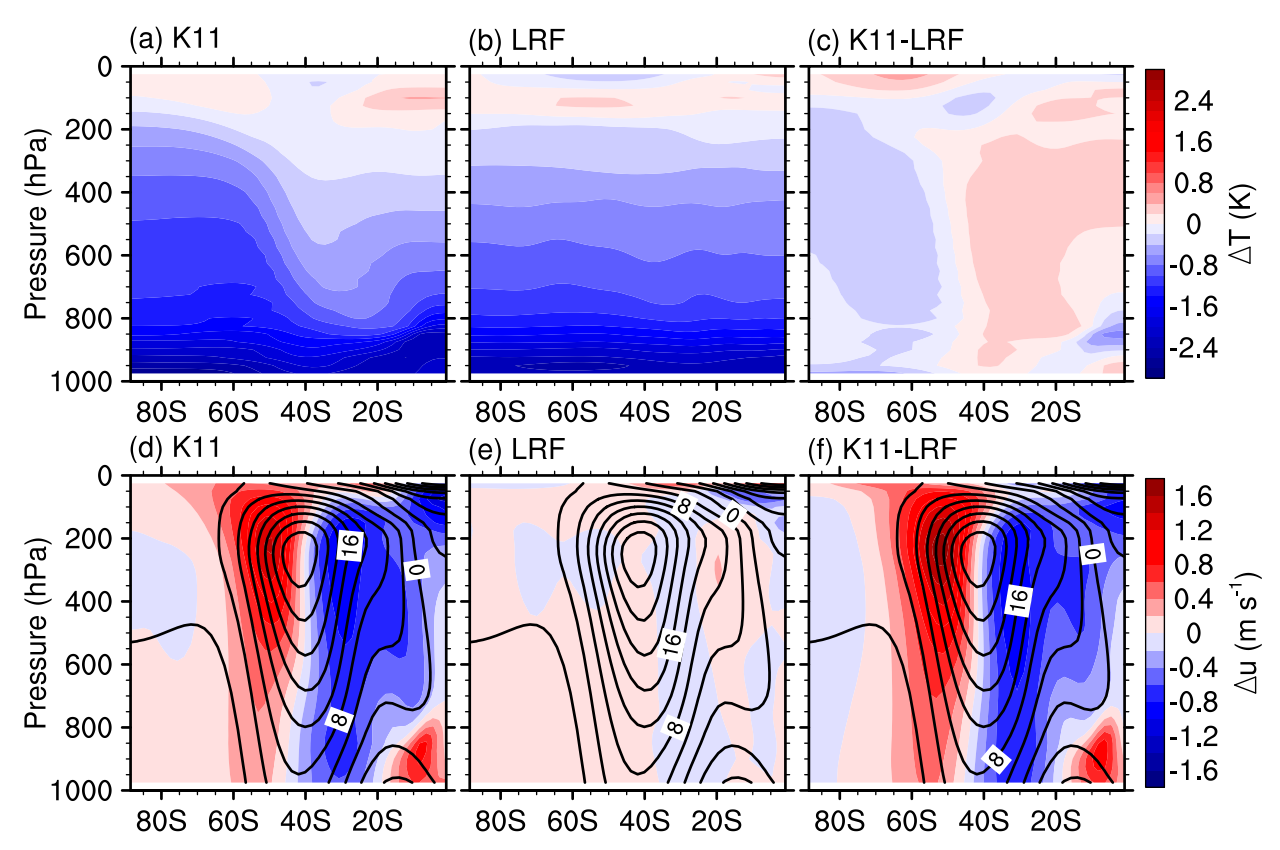


FIG. 1. Mean (a)–(c) temperature change and (d)–(f) zonal wind change in experiments (left) K11, (middle) LRF, and (right) K11–LRF. Contours in (d)–(f) show the climatological zonal wind in the control experiment.

LRF: This experiment targets a mean state with increased static stability without changing meridional temperature gradient, by applying a time-invariant and zonally uniform forcing (see section 2c). The temperature part of this target mean-state change is set to the meridional average of the temperature change in experiment K11 (around 2 K decrease near surface). The zonal wind part of this target mean-state change is set to zero.

K11–LRF: This experiment is K11 minus LRF, which applies the forcing in K11 plus the opposite forcing in experiment LRF. This experiment helps explain the difference in results from the two experiments of increased static stability. If the mean-state change is linear to the forcing applied, the meridional temperature gradient will change without changing the mean static stability.

 $0.5 \times LRF$, $-0.5 \times LRF$, $-1.0 \times LRF$: These are 3 more experiments with 0.5, -0.5, and -1.0 times the forcing in experiment LRF.

c. Iterative use of linear response function

The above-mentioned experiment LRF needs to find a time-invariant and zonally uniform forcing to force a target mean-state change. Being time-invariant and zonally uniform, the forcing does not directly act on the eddies. Some previous approaches (e.g., Yuval and Kaspi 2020) do not have this merit.

We find the forcing by iterative use of a LRF matrix as follows. For a state vector $\overline{\mathbf{x}}$ consisting of zonal mean temperature and zonal wind, a LRF matrix L is a square matrix that linearly relates the target mean-state change $\overline{\mathbf{x}}_{target}$ and the required forcing $\bar{\mathbf{f}}_1$, as $\bar{\mathbf{f}}_1 = -\mathbf{L}\bar{\mathbf{x}}_{\text{target}}$. A LRF matrix \mathbf{L} of this dry GCM was constructed by Hassanzadeh and Kuang (2016) following the framework in Kuang (2010) using Green's functions. That is to run the GCM multiple times, each time with only one element of the forcing vector $\bar{\mathbf{f}}$ being nonzero, and quantify the equilibrated change in state vector $\overline{\mathbf{x}}$. Solving the equation $\mathbf{F} = -\mathbf{L}\mathbf{X}$ via matrix inversion, where \mathbf{F} and \mathbf{X} are $\overline{\mathbf{f}}$ and $\overline{\mathbf{x}}$ assembled into square matrices, will give us matrix L [see Hassanzadeh and Kuang (2016) for details]. Having the LRF matrix \mathbf{L} , the first iteration uses forcing $\overline{\mathbf{f}}_1 = -\mathbf{L}\overline{\mathbf{x}}_{target}$ and produces a mean-state change $\overline{\mathbf{x}}_1$. Because the LRF matrix is not perfect, $\overline{\mathbf{x}}_1$ may not be as close to $\overline{\mathbf{x}}_{\text{target}}$ as needed. The *n*th iteration takes forcing $\bar{\mathbf{f}}_n = \bar{\mathbf{f}}_{n-1} - \mathbf{L}(\bar{\mathbf{x}}_{\text{target}} - \bar{\mathbf{x}}_{n-1})$ and produces a mean-state change $\overline{\mathbf{x}}_n$. In our case, the second iteration gives a satisfactory mean state as shown later.

d. Mean state

Our K11 experiment reproduces the mean-state change in the $N_{\rm increased}$ experiment in Kidston et al. (2011) reasonably well (Fig. 1). The experiment comes with a noticeably increased meridional temperature gradient around 50°S. According to the thermal wind balance, such change in meridional temperature

gradient will give rise to change in zonal wind. Hereafter, we quantify the change in zonal wind as an indirect measure of meridional temperature gradient. The change of zonal wind reaches around $1.4\,\mathrm{m\,s^{-1}}$ in experiment K11. Such changes in meridional temperature gradient and zonal wind make it hard to attribute the response of eddies solely to the increased N.

Our LRF experiment targets a mean state with increased N without changing meridional temperature gradient. The experiment successfully produces much weaker change in meridional temperature gradient. And the zonal wind is also close to our target of zero change—mostly the change is less than $0.2\,\mathrm{m\,s^{-1}}$ except near the model top (Fig. 1). We note that with our $1\,000\,000$ -day-equivalent ensembles, the $95\,\%$ confidence interval of the difference between two ensembles is smaller than $0.14\,\mathrm{m\,s^{-1}}$ for zonal wind (not shown). This very narrow confidence interval is helpful to the success of getting a small change in meridional temperature gradient, especially when we are using an iterative approach.

Experiment K11–LRF has its mean-state change roughly equal to the difference between K11 and LRF, which changes meridional temperature gradient without changing the mean static stability (Fig. 1). This indicates that the mean state depends approximately linearly on the forcing.

e. Spectral decomposition

We decompose zonal and meridional winds u and v into zonal spectra \tilde{U}_k and \tilde{V}_k . The value of $\overline{v'^2}$ at zonal wavenumber k is calculated as $0.5 \times |\tilde{V}_k|^2$, and likewise for $\overline{u'^2}$.

Following Chemke and Kaspi (2016), we define energy-containing zonal wavenumber k_e (at each latitude ϕ) as the "squared inverse centroid" of the zonal spectrum of barotropic $\overline{v^2}$ as follows:

$$k_e^{-2} = \frac{\sum_{k} k^{-2} |\tilde{V}_k|^2}{\sum_{k} |\tilde{V}_k|^2},\tag{4}$$

and the energy-containing zonal scale L_e is $2\pi a \cos\phi/k_e$, where a is Earth's radius. To decompose momentum flux in zonal phase speeds (Randel and Held 1991), we first decompose u and v at every 100-day slot into zonal wavenumber–frequency spectra $\tilde{U}_{k,\omega}$ and $\tilde{V}_{k,\omega}$. The value of $\overline{u'v'}$ at zonal wavenumber k and frequency ω is calculated as $0.5 \times \text{Re}[\tilde{U}_{k,\omega} \, \tilde{V}_{k,\omega}^*]$, where the asterisk (*) denotes the complex conjugate. Then the zonal wavenumber–frequency spectrum of $\overline{u'v'}$ is averaged across different 100-day slots and different ensemble members. Next, notice that angular phase speed $c/\cos\phi = \omega a/k$. We use a 1 m s^{-1} bin size in angular phase speed and sum up the proportionate spectrum according to the fraction of (k, ω) grid giving $c - 0.5 \le \omega a/k < c + 0.5$.

The momentum flux convergence is calculated like Eq. (9) in Kidston et al. (2011):

$$-\frac{1}{a\cos^2\phi} \frac{\partial}{\partial\phi} \bigg|_{c/\cos\phi} \overline{u'v'} \cos^2\phi. \tag{5}$$

Afterward, this flux convergence is plotted as a function of intrinsic angular phase speed $(c - \overline{u})/\cos\phi$.

f. Maximum baroclinic growth scale

The maximum baroclinic growth scale L_{grow} is calculated using the linear baroclinic instability calculation code that is described in Pfahl et al. (2015, p. 9381). Briefly, the code solves the linearized QG potential vorticity equation in pressure coordinate as an eigenvalue problem. The code inputs vertical profiles of zonal wind and thermal stratification from the mean state of the GCM. For boundary conditions, the vertical velocity in pressure coordinate is zero at the model top (0 hPa) and the vertical velocity in height coordinate is set to zero at the surface. We adapt the Rayleigh damping of lowlevel winds in the code to be the same rate as the GCM, with maximum drag coefficient of 1 day⁻¹ (Held and Suarez 1994). Newtonian relaxation of temperature is not applied. The meridional wavenumber is set to zero. For each k, the code calculates a vector of complex eigenvalues (the real part is the growth rate and the imaginary part is the frequency) and outputs the complex eigenvalue with the largest positive real part. The k outputting eigenvalue with the largest positive real part will give us the maximum baroclinic growth scale $L_{\rm grow}$.

g. Rossby radius and Rhines scale

The Rossby radius is calculated as Eq. (1). The H in Eq. (1) is the tropopause height calculated as the height where the static stability N reaches $0.015 \, \mathrm{s}^{-1}$ (Chemke and Kaspi 2016). Similar to Chemke and Kaspi (2016) and Frierson et al. (2006), the static stability N in Eq. (1) is the vertical average below the tropopause height, i.e., $N = \sqrt{g(\ln\theta_{\rm trop} - \ln\theta_{\rm bot})/H}$, with $\theta_{\rm trop}$ being the potential temperature at the tropopause and $\theta_{\rm bot}$ being the potential temperature at the lowest level.

The Rhines scale is calculated as Eq. (2), where EKE is calculated as the vertically averaged $(1/2)(u^{7/2} + \overline{v^{7/2}})$ (similar to Chemke and Kaspi 2016).

3. Results

a. Eddy spectra

In experiment K11, we qualitatively reproduce results in Kidston et al. (2011) that the zonal scale of eddies increases, and eddies shift poleward (Fig. 2a).

In our LRF experiment, we find EKE decreases at every zonal wavenumber and latitude (Fig. 2b). Stronger decrease happens at smaller zonal wavenumbers, causing a decreased eddy zonal scale. This decreasing zonal scale is opposite to that of experiment K11, suggesting that the change in meridional temperature gradient is important in controlling the eddy length scale and played a role in the conclusion of Kidston et al. (2011). It is clearer in experiment K11-LRF, which only increases meridional temperature gradient without changing the mean static stability. The increase in meridional temperature gradient causes a strong increase of EKE at small zonal wavenumbers. It dominates over the effect of increased static stability and causes the eddy zonal scale to increase in experiment K11. Here the EKE response in experiment K11 is roughly the sum of those in LRF and K11-LRF, suggesting that this is roughly linear to the forcing added.

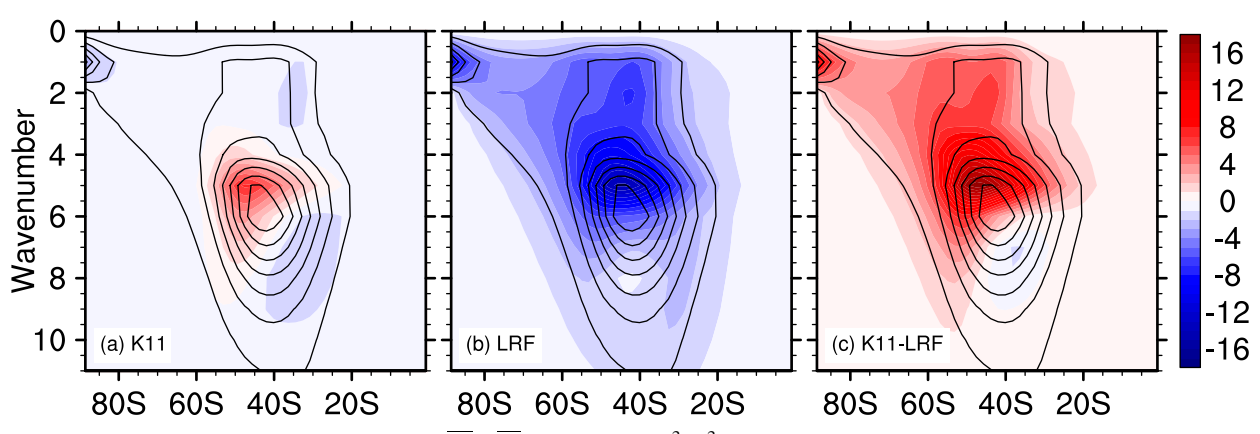


FIG. 2. Changes in the zonal spectra of $(1/2)(\overline{u'^2} + \overline{v'^2})$ at 300 hPa (m² s⁻²) in experiments (a) K11, (b) LRF, and (c) K11–LRF. Black contours show the spectra in the control experiment at intervals of 10.

In their study of the jet's poleward shift under climate change, Kidston et al. (2011) proposed that an increase of static stability will increase the eddy length scale, which will make the intrinsic phase speed of eddies more negative, i.e., westward. In this line of thought, Fig. 3 is more relevant, which plots momentum flux convergence as a function of intrinsic angular phase speed and latitude, following Fig. 6 in Kidston et al. (2011). In experiment K11, like the zonal spectrum of EKE (Fig. 2a), the momentum flux convergence shifts poleward and to more negative intrinsic phase speed (Fig. 3a). In experiment LRF, in contrast, momentum flux convergence does not shift meridionally but shifts to less negative phase speed (Fig. 3b). So increased wavenumber of EKE in Fig. 2b indeed corresponds to less negative phase speed of momentum flux convergence. In experiment K11-LRF, there is a stronger shift, poleward and toward more negative (westward) intrinsic phase speed (Fig. 3c).

b. Evaluating eddy-length-scale theories

Now, let us compare different length scale arguments in experiment LRF. The actual energy-containing zonal scale decreases by around 3% to 4%, which matches with Rhines

scale near the jet core (Fig. 4a). When forcing is applied in different signs and magnitudes, similar behaviors are found (Fig. 4b). Therefore, the results here are robust.

The Rossby radius in experiment LRF increases by around 2%, which is opposite to the observed decrease of the energy-containing zonal scale L_e (Fig. 4a).

The maximum baroclinic growth scale in experiment LRF decreases by around 1% (Fig. 4a), which is less than the observed decrease of L_e . By accounting for the nonuniform profile of static stability and zonal wind, this scale goes in the opposite direction to static stability or the Rossby radius. The difference between this scale and the Rossby radius is also noted by Chemke and Kaspi (2016). Note that even more ideally, the maximum baroclinic growth scale should be calculated globally accounting for meridional variations, rather than locally at each latitude.

The Rhines scale in experiment LRF decreases by around 4%-8% (Fig. 4a). It matches well with the observed change of L_e near the jet core. Away from the jet (or latitude of maximum EKE), the Rhines scale decreases more than the observed eddy length scale. This is somewhat consistent with Frierson et al. (2006), who found the Rhines scale at the latitude of maximum

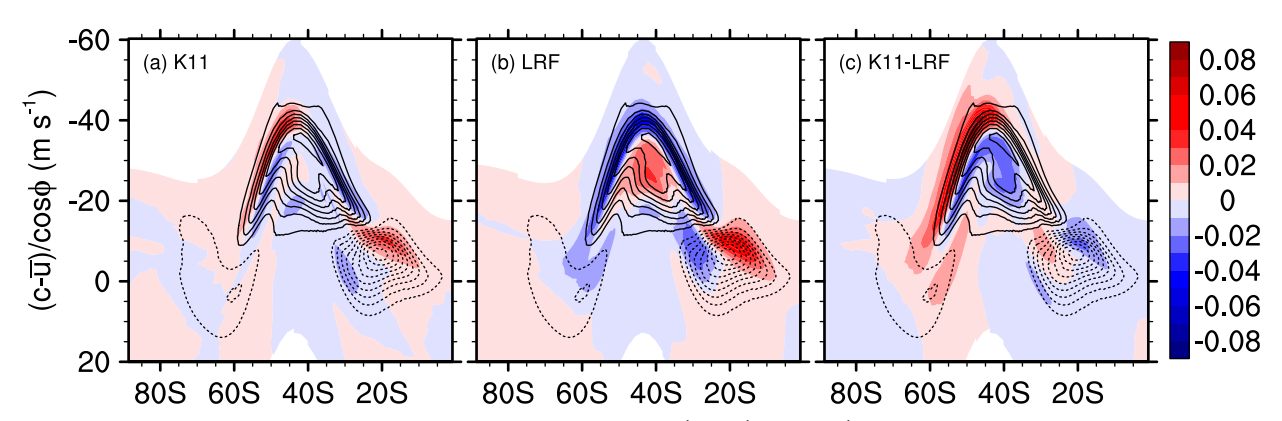


FIG. 3. Changes in the momentum flux convergence at 300 hPa (m s $^{-1}$ day $^{-1}$ per m s $^{-1}$ bin), as a function of intrinsic angular phase speed and latitude, in experiments (a) K11, (b) LRF, and (c) K11–LRF. Black contours show the momentum flux convergence (solid) and divergence (dotted) in the control experiment at intervals of 0.025.

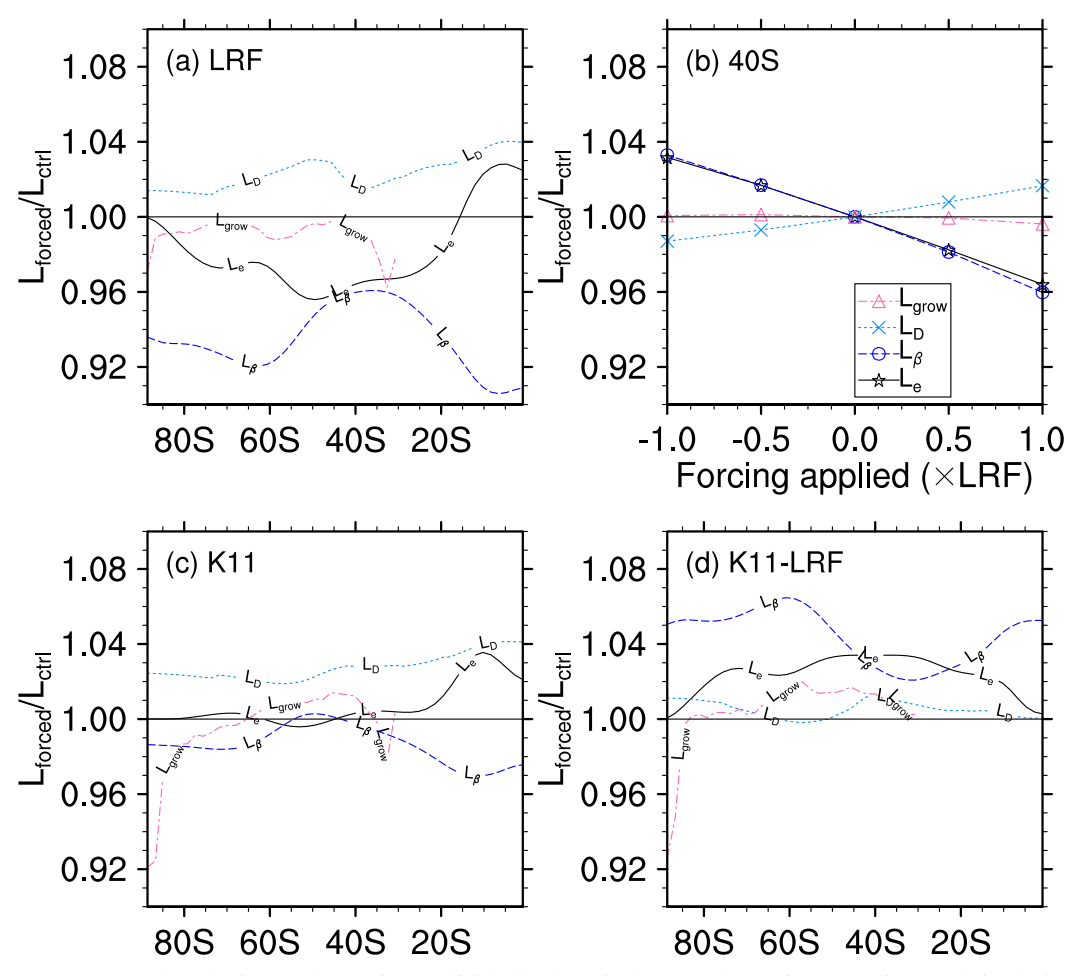


FIG. 4. Length scales in forced experiments divided by those in the control experiment: at different latitudes in experiments (a) LRF, (c) K11, and (d) K11–LRF, and (b) at 40°S in different experiments. Shown are the energy-containing zonal scale L_e , the Rhines scale L_β , the Rossby radius L_D , and the maximum baroclinic growth scale $L_{\rm grow}$. The Kuo scale L_K is not shown. The maximum baroclinic growth scale $L_{\rm grow}$ is not shown equatorward of 30°S where it starts to jump between different branches of unstable scales.

EKE to work better than the local Rhines scale. The latter was too sensitive to moisture content in their moist GCM. One way to think about the bad performance of the Rhines scale at latitudes away from the jet core is that the Rhines scale was originally derived in a spatially uniform setting. When away from the jet core, fewer eddies originate locally and more come from other latitudes. Assumption of uniform setting fails and so does the Rhines scale at latitudes away from the jet core. Also, note that the Rhines scale changes in the opposite direction as the Rossby radius does, and this is in contrast to the findings of Schneider and Walker (2006), who suggested that the Rhines scale and the Rossby radius change in the same way and cannot be separated. Such inconsistency with the findings of Schneider and Walker (2006) was observed in previous studies (e.g., Zurita-Gotor 2008; Jansen and Ferrari 2012) because the isentropic slope does not remain constant.

The Kuo scale in experiment LRF remains basically unchanged (not shown), as the mean zonal wind in this experiment remains basically unchanged. The Kuo scale does not agree with the observed decrease in L_e .

As a supplement to analyses of experiment LRF, we note that in experiments K11 and K11–LRF, the observed changes of L_e also match with the Rhines scale near the jet core, but not the Rossby radius (Figs. 4c,d).

4. Conclusions and discussion

With iterative use of the LRF of an idealized dry GCM, we are able to increase the static stability with very small change in the meridional temperature gradient and zonal wind, by a time-invariant and zonally uniform forcing. The change in meridional temperature gradient, as measured by change in zonal wind, is mostly less than 0.2 m s⁻¹ when temperature near surface is cooled by more than 2 K (Figs. 1b,e). In this well-controlled experiment, the energy-containing zonal scale decreases with increased static stability (Figs. 2b, 4a). We also find momentum flux convergence to shift toward less negative intrinsic phase speed (Fig. 3b), consistent with a decreased length scale. This is against the argument of Kidston et al. (2011)

and the Rossby radius as eddy length scale, which would predict length scale to increase with static stability.

In this well-controlled experiment, we also quantitatively tested the applicability of several length scale arguments. In experiment LRF (around 2 K decrease near surface), we find energy-containing zonal scale to decrease by around 3% to 4%, which matches well with the Rhines scale near the jet core. The Rossby radius (+2%), the maximum baroclinic growth scale (-1%), and the Kuo scale (0%) do not match the observed change in eddy length scale. Additional controlled experiments in which the sign and/or magnitude of the forcing are changed further confirm that the zonal eddy length scale varies linearly with the Rhines scale (Fig. 4b).

Here our focus is the statistics of equilibrated eddies. Nonequilibrated eddies may not respond to static stability in the same way we see here. Therefore, our results may not apply to internal variability of eddy length scale, which is also analyzed by Kidston et al. (2011).

Our well-controlled experiment of increased static stability without changing the mean zonal wind may also be used to analyze other statistics of equilibrated eddies, for example, on how they transport momentum and heat. One might notice that in experiment LRF, EKE decreases at all zonal wavenumbers (Fig. 2b), while momentum flux convergence locally strengthens at some intrinsic phase speeds and latitudes (Fig. 3b). This could suggest a more efficient momentum transport per EKE in this experiment and is being studied in future work.

Our framework of forcing a mean state can further be applied to more realistic models such as an idealized moist GCM, in which we can see the effect of moisture.

Acknowledgments. The computations in this paper were run on the FASRC Cannon cluster supported by the FAS Division of Science Research Computing Group at Harvard University. The authors thank Paul O'Gorman, Ebrahim Nabizadeh, Brian Farrell, Peter Huybers, Eli Tziperman, Wanying Kang, Duo Chan, and Lei Wang for fruitful discussions. We are grateful to three anonymous reviewers for insightful feedbacks. This work was supported by NSF Grant AGS-1552385, NASA Grant 80NSSC17K0267, and a grant from the Harvard Global Institute (to Z. K.), and NSF Grant AGS-1921413 (to P. H.). This paper is substantially based on the first author's Ph.D. dissertation (Chan 2020).

Data availability statement. The linear baroclinic instability code is provided by Paul O'Gorman. The GFDL dry spectral dynamical core can be acquired from https://www.gfdl.noaa.gov/idealized-spectral-models-quickstart/. The NCAR Command Language is obtained from https://doi.org/10.5065/D6WD3XH5. Data displayed in this paper are available from https://github.com/PackardChan/chk2021-lengthscale-dry.

REFERENCES

- Barry, L., G. C. Craig, and J. Thuburn, 2002: Poleward heat transport by the atmospheric heat engine. *Nature*, **415**, 774–777, https://doi.org/10.1038/415774a.
- Chan, P. W., 2020: Evaluating blocking indices and investigating eddies' response to static stability. Ph.D. thesis, Harvard

- University, 128 pp., https://search.proquest.com/docview/2467866555.
- Chemke, R., and Y. Kaspi, 2016: The effect of eddy-eddy interactions on jet formation and macroturbulent scales. *J. Atmos. Sci.*, **73**, 2049–2059, https://doi.org/10.1175/JAS-D-15-0375.1.
- Farrell, B. F., and P. J. Ioannou, 2007: Structure and spacing of jets in barotropic turbulence. *J. Atmos. Sci.*, **64**, 3652–3665, https://doi.org/10.1175/JAS4016.1.
- Frierson, D. M. W., I. M. Held, and P. Zurita-Gotor, 2006: A gray-radiation aquaplanet moist GCM. Part I: Static stability and eddy scale. J. Atmos. Sci., 63, 2548–2566, https://doi.org/10.1175/JAS3753.1.
- Hassanzadeh, P., and Z. Kuang, 2016: The linear response function of an idealized atmosphere. Part I: Construction using Green's functions and applications. *J. Atmos. Sci.*, 73, 3423–3439, https://doi.org/10.1175/JAS-D-15-0338.1.
- Held, I. M., and M. J. Suarez, 1994: A proposal for the intercomparison of the dynamical cores of atmospheric general circulation models. *Bull. Amer. Meteor. Soc.*, 75, 1825–1830, https://doi.org/10.1175/1520-0477(1994)075<1825:APFTIO>2.0.CO;2.
- —, and V. D. Larichev, 1996: A scaling theory for horizontally homogeneous, baroclinically unstable flow on a beta plane.
 J. Atmos. Sci., 53, 946–952, https://doi.org/10.1175/1520-0469(1996)053<0946:ASTFHH>2.0.CO;2.
- Jansen, M., and R. Ferrari, 2012: Macroturbulent equilibration in a thermally forced primitive equation system. J. Atmos. Sci., 69, 695–713, https://doi.org/10.1175/JAS-D-11-041.1.
- Kang, W., M. Cai, and E. Tziperman, 2019: Tropical and extratropical general circulation with a meridional reversed temperature gradient as expected in a high obliquity planet. *Icarus*, 330, 142–154, https://doi.org/10.1016/j.icarus.2019.04.028.
- Kidston, J., S. M. Dean, J. A. Renwick, and G. K. Vallis, 2010: A robust increase in the eddy length scale in the simulation of future climates. *Geophys. Res. Lett.*, 37, L03806, https:// doi.org/10.1029/2009GL041615.
- —, G. K. Vallis, S. M. Dean, and J. A. Renwick, 2011: Can the increase in the eddy length scale under global warming cause the poleward shift of the jet streams? *J. Climate*, 24, 3764–3780, https://doi.org/10.1175/2010JCLI3738.1.
- Kuang, Z., 2010: Linear response functions of a cumulus ensemble to temperature and moisture perturbations and implications for the dynamics of convectively coupled waves. *J. Atmos. Sci.*, 67, 941–962, https://doi.org/10.1175/2009JAS3260.1.
- Nabizadeh, E., P. Hassanzadeh, D. Yang, and E. A. Barnes, 2019: Size of the atmospheric blocking events: Scaling law and response to climate change. *Geophys. Res. Lett.*, 46, 13 488–13 499, https://doi.org/10.1029/2019GL084863.
- Panetta, R. L., 1993: Zonal jets in wide baroclinically unstable regions: Persistence and scale selection. *J. Atmos. Sci.*, **50**, 2073–2106, https://doi.org/10.1175/1520-0469(1993) 050<2073:ZJIWBU>2.0.CO;2.
- Pfahl, S., P. A. O'Gorman, and M. S. Singh, 2015: Extratropical cyclones in idealized simulations of changed climates. *J. Climate*, 28, 9373–9392, https://doi.org/10.1175/JCLI-D-14-00816.1.
- Randel, W. J., and I. M. Held, 1991: Phase speed spectra of transient eddy fluxes and critical layer absorption. *J. Atmos. Sci.*, **48**, 688–697, https://doi.org/10.1175/1520-0469(1991) 048<0688:PSSOTE>2.0.CO:2.
- Rhines, P. B., 1975: Waves and turbulence on a beta-plane. J. Fluid Mech., 69, 417–443, https://doi.org/10.1017/S0022112075001504.
- Schneider, T., and C. C. Walker, 2006: Self-organization of atmospheric macroturbulence into critical states of weak nonlinear eddy-eddy interactions. *J. Atmos. Sci.*, 63, 1569–1586, https://doi.org/10.1175/JAS3699.1.

- —, T. Bischoff, and H. Płotka, 2015: Physics of changes in synoptic midlatitude temperature variability. *J. Climate*, 28, 2312–2331, https://doi.org/10.1175/JCLI-D-14-00632.1.
- Smith, K. S., 2007: The geography of linear baroclinic instability in Earth's oceans. J. Mar. Res., 65, 655–683, https://doi.org/ 10.1357/002224007783649484.
- Thompson, A. F., and W. R. Young, 2007: Two-layer baroclinic eddy heat fluxes: Zonal flows and energy balance. *J. Atmos. Sci.*, **64**, 3214–3231, https://doi.org/10.1175/JAS4000.1.
- Vallis, G. K., 2006: Atmospheric and Oceanic Fluid Dynamics: Fundamentals and Large-Scale Circulation. Cambridge University Press, 745 pp.
- Yuval, J., and Y. Kaspi, 2020: Eddy activity response to global warming-like temperature changes. J. Climate, 33, 1381–1404, https://doi.org/10.1175/JCLI-D-19-0190.1.
- Zurita-Gotor, P., 2008: The sensitivity of the isentropic slope in a primitive equation dry model. *J. Atmos. Sci.*, **65**, 43–65, https://doi.org/10.1175/2007JAS2284.1.